Pergamon

Cement and Concrete Research, Vol. 28, No. 5, pp. 699–711, 1998

0008-8846/98 $19.00 + .00

PII S0008-8846(98)00037-4

RELATIONSHIP BETWEEN PORE STRUCTURE AND MECHANICAL PROPERTIES OF ORDINARY CONCRETE UNDER BENDING FATIGUE

B. Zhang
Department of Civil Engineering, University of Glasgow, Glasgow G12 8LT, Scotland, UK

(Received July 8, 1997; in final form March 5, 1998)

ABSTRACT

Progressive macro damage of concrete under fatigue loading is caused by the change of its internal micro-meso properties such as pore structure. In this study, porosity, pore size distribution, and specific surface area of ordinary concrete at different fatigue stages were investigated using mercury intrusion, helium flow, and nitrogen adsorption (BET) methods. These properties changed with increasing loading cycles and could be taken as micro-meso damage parameters to evaluate macro fatigue damage of concrete. Test results showed that both porosity in mortar (mainly macro pores) and interface between mortar and coarse aggregates (interfacial cracks) developed at a similar rate. The corresponding residual bending fatigue strength and dynamic bending Young's modulus were also obtained and their relationships with these micro-meso properties were established. The "intrinsic bending strength" and "intrinsic bending Young's modulus" were predicted from these relationships. © *1998 Elsevier Science Ltd*

Introduction

Concrete under repeated loading sustains a gradual fatigue damage. At macro level, strength and Young's modulus decrease with increasing loading cycles (1–3); at micro-meso level, internal structures degenerate and micro-defects (pores, cracks, etc.) develop. The investigation on micro-meso properties of concrete helps to understand the mechanisms of macro fatigue damage and possibly to find ways to improve the fatigue resistance of concrete. Pore structure is an important micro-meso property which determines macro properties of concrete such as strength (4–10), elasticity (4–6,10), shrinkage (11), durability (12–15), etc. Cement paste, mortar, and concrete are all porous materials. Any change in pore structure may lead to sharp changes in performance.

Concrete science classifies structural levels as micro ($\leq$1 μm), meso (1 μm to 1 cm), and macro ($>$1 cm). Internal structures of concrete imply those at micro and meso levels. At micro level, structures are discontinuous and inhomogeneous such as molecular and crystal structures, gels and pores; at meso level, structures are continuous but inhomogeneous such as coarse and fine aggregates, cement hydrates, unhydrated cement particles, pores, and interface; at macro level, concrete is continuous and homogenous. Pore structure is a parameter which relates all three structural levels. It includes porosity, pore size distribution

and specific surface area. Pores can be clarified as micro pores (≤25 Å), meso pores (25–500 Å), macro pores (500 Å–10 μm), and air voids (>10 μm) (14).

In the past 30 years, a lot of experimental work has been done to investigate the effects of pore structure on macro properties of cement paste, mortar, and concrete (1–15). There are good correlations between pore structure, mechanical properties (compressive and flexural strength, elastic modulus, and toughness), and durability (permeability, frost resistance, etc.). Typical strength-porosity relationships that have been widely used for concrete materials are:

$$f = f_0(1 - P)^{k_1} \quad \text{(ref. 16)} \tag{1}$$

$$f = f_0 \exp(-k_2 P) \quad \text{(ref. 17)} \tag{2}$$

$$f = k_3 \ln(P_0/P) \quad \text{(ref. 18)} \tag{3}$$

$$f = f_0 - k_4 P \quad \text{(refs. 19 and 20)} \tag{4}$$

where f is strength, f_0 is strength at zero porosity or the intrinsic strength, P is porosity, P_0 is porosity at zero strength, and k_1, k_2, k_3, and k_4 are constants. Similar elastic modulus or hardness versus porosity relations have been used (6,10) Actually, concrete strength depends on not only porosity but also pore size distribution. Odler and Rößler (21) proposed a multi-linear function:

$$f = f_0 - k_{10}P_{<10\text{nm}} - k_{20}P_{10-100\text{nm}} - k_{30}P_{>100\text{nm}} \tag{5}$$

where $P_{<10\text{nm}}$, $P_{10-100\text{nm}}$, and $P_{>100\text{nm}}$ are porosities for different pore size ranges, and k_{10}, k_{20}, and k_{30} are constants. Atzeni et al. (22) introduced a mean distribution pore radius r_m as:

$$\ln r_m = (\Sigma P_i \ln r_i)/(\Sigma P_i) \tag{6}$$

where P_i is the porosity at pore radius r_i. Equation 6 considers the "weighted" pore size distribution of every pore class involved. They proposed a formula to relate strength to P and r_m as:

$$f = Kf_0(1 - P)/\sqrt{r_m} \tag{7}$$

where K is a constant. From Griffith's approach and subsequent modifications (23), r_m can be regarded as a statistically equivalent size of macro defect, so it can be related to macro mechanical properties of materials. Using Weibull's strength distribution theory (24), Ding (25) obtained a relationship of the compressive strength of hardened cement paste with total porosity and specific surface area as:

$$f = K_1 \frac{1 - P}{1 + 2P} [K_2(1 - P)]^{K_3 S + K_4} \tag{8}$$

where K_1, K_2, K_3, and K_4 are constants and S is specific surface area. Huang et al. (26) rearranged the above equation as:

$$f = A \cdot B(P) \cdot C(P) = [K_1 K_2^{K_3 + K_4}][K_2^{K_3(S-1)}(1 - P)^{K_3 S + K_4}]\left[\frac{1 - P}{1 + 2P}\right] \tag{9}$$

where $A = K_1 K_2^{K_3+K_4}$ stands for the internal strength at atom-molecule level which depends on properties and arrangements of solid phases but is independent of porosity; $B(P) =$

TABLE 1
Mix design of concrete.

Material	Cement	Water	Fine Aggregate	Coarse Aggregate
Type	#525 OPC	Tap water	Natural river sand	15 mm graded gravel
Ratio	1	0.45	1.18	2.47
Content (kg/m^3)	456	205	538	1251

$K_2K_2^{K_3(S-1)}(1-P)^{K_3S+K_4}$ expresses the effect of micro pores on stress distribution of multi-phase materials; $C(P) = (1-P)/(1+P)$ expresses the effect of micro-meso pores.

Very few papers have been published about the development of concrete porosity under loading. Pons and Maso (27) measured porosity of cement paste after uniaxial compressive loading cycles at low frequencies and found that these loading cycles were not liable to damage or micro-crack concrete but to strengthen and consolidate it. So far no researchers have dealt with porosity development under cyclic tensile or flexural loading.

In this paper, mercury intrusion, helium flow, and nitrogen adsorption (BET) methods are used to measure porosity, pore size distribution, and specific surface area of ordinary concrete at different bending fatigue stages. These properties can be used as micro-meso damage parameters to help to understand the mechanisms of macro fatigue damage and failure and to find possible ways to improve fatigue resistance of concrete. The relationships between these micro-meso properties and the corresponding mechanical properties can be established. Thus, the "intrinsic strength" and "intrinsic bending Young's modulus" can be predicted using extrapolation.

Experimental Investigations

Test Specimens

Samples for micro-meso tests were cut from the maximum tensile zone of concrete beams of 500 × 100 × 100 mm which sustained cyclic bending. After certain loading cycles, they were tested to determine the residual strength and stiffness. The mix design is listed in Table 1. Specimens were cured in the curing room for 28 days, at 20 ± 2°C and relative humidity of 90%, before they were moved outdoors. At 90 days, these specimens were used for flexural tests, because by then the strength and stiffness of concrete would change very little. Material properties of concrete are listed in Table 2, including the compressive strength f_c', modulus of rupture f_r, Young's modulus E, and Poisson's ratio v at 28 and 90 days.

TABLE 2
Material properties of concrete.

28 days		90 days						
f_c' (MPa	f_r (MPa)	f_c' (MPa)	f_r (MPa)	E (GPa)	E_{dB} (GPa)	v	v_d	G_d (GPa)
50.7	7.19	57.4	7.88	41.1	46.2	0.17	0.23	18.9

A total of 40 specimens were subjected to third-point bending cyclic loading with an effective span of 450 mm in a 250 kN Instron servo testing machine. Before these tests, all specimens were non-destructively detected to determine the dynamic stiffness parameters say the dynamic Young's modulus E_{dB}, the dynamic Poisson's ratio v_d, and the dynamic shear modulus G_d (Table 2). In the cyclic tests, the stress level was 70.6% f_r and the stress ratio was 0.2 with a sinusoidal waveform and a loading frequency of 20 Hz. Thus the corresponding fatigue life N was calculated as 2×10^5 (1). Thirty-two specimens were tested to determine the residual fatigue strength and stiffness properties at different fatigue stages and the remaining eight plus two undamaged beams were used to determine the micro-meso properties of concrete.

Mercury Intrusion

Porosity and pore size distribution of the damaged concrete under cyclic bending and the undamaged concrete were measured using a high-pressure mercury intrusion porosimeter. The maximum pressure of the porosimeter was 250 MPa. The measurable pore size (radius r) was between 40Å to 75000Å. Values of 0.480 N/m and 140° were used for the surface tension of mercury and the wetting angle.

After certain designed loading cycles N_1, a diamond saw was used to cut out 10 to 20 mm high samples. Due to the limitation of sample size for the porosimeter, original concrete could no longer be used so only the mortar without coarse aggregate was picked out to measure the pore volume P_m. Seven out of the ten samples were taken during middle fatigue stages, one at failure and the remaining two were from the undamaged concrete as references. Typical pore size distribution results (dP_m/d log r vs. log r) at different fatigue stages are shown in Figure 1. The corresponding cumulative pore volume P_{m0} vs. log r relationships are shown in Figure 2.

Helium Flow

As mercury intrusion tests were conducted, helium flow method was used on larger samples to measure the porosity from the corresponding specimens. Two concrete samples of $20 \times 20 \times 10$ mm from the same specimen were used for each test. A total of ten sets of test data were obtained.

Nitrogen Adsorption (BET)

Nitrogen adsorption method was used to measure specific surface area of concrete. Only the mortar was picked out from the original damaged concrete for the BET tests due to the limitation of sample size. Three samples were tested.

Residual Fatigue Properties

It is impossible to measure the residual strength and micro-meso properties on the same specimen. The residual strength f_{cr} is predicted using the previously proposed formula (1). The residual dynamic Young's modulus E_{dB} was non-destructively measured using a dy-

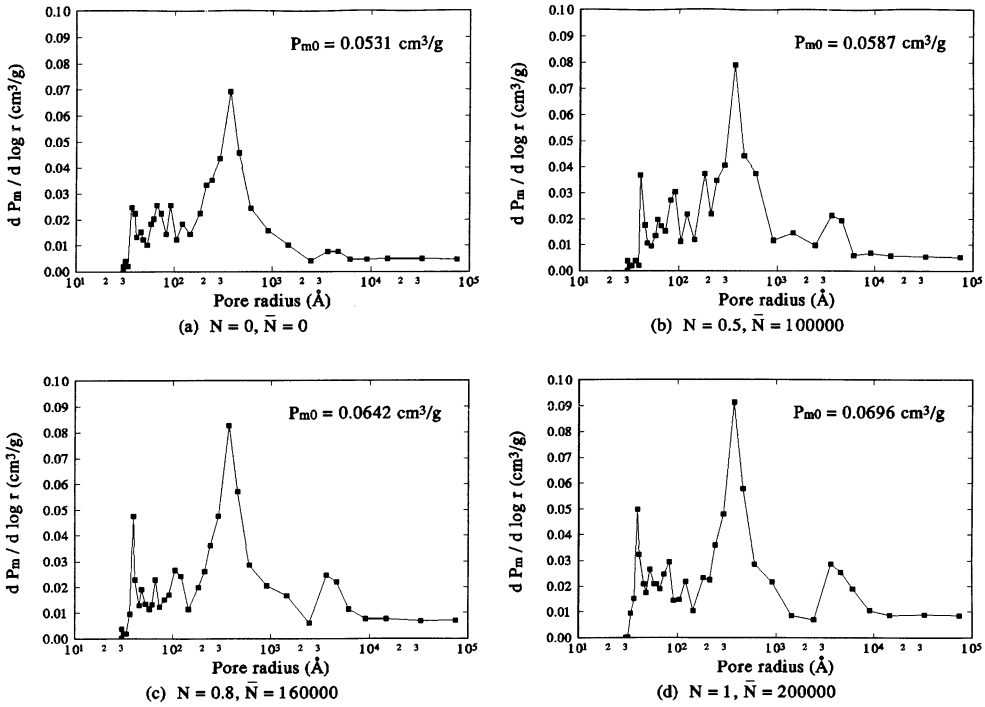

FIG. 1.
Pore size distribution of mortar (concrete) at different fatigue stages.

namic elastic parameter instrument based on resonance mechanism (1) before samples were cut from the specimen. The calculated relative residual fatigue strength f_{cr} and the measured relative dynamic Young's modulus $\bar{E}_{dB}$ are the ratios of the values at different fatigue stages to those from undamaged specimens.

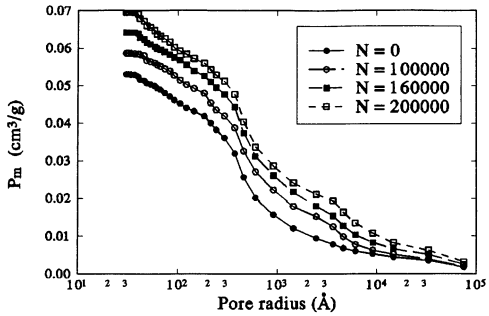

FIG. 2.
Cumulative pore volume of mortar (concrete) at different fatigue stages.

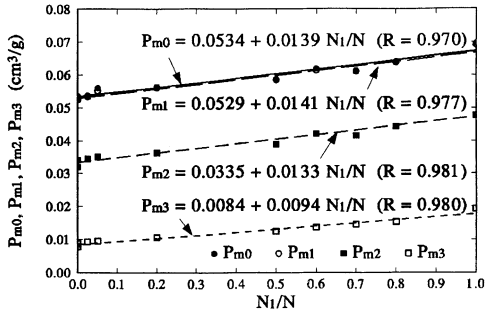

FIG. 3.
Typical pore volumes of mortar (concrete) at different fatigue stages.

Development of Micro-Meso Parameters Under Bending Fatigue

Porosity of Mortar Using Mercury Intrusion P_{m0}

In micro-meso damage mechanics, porosity can be used as a damage parameter to evaluate the fatigue damage state of concrete. Figure 3 shows that the porosity of mortar P_{m0} very linearly increased with increasing loading cycles N_1/N until final fatigue stage. When $N_1/N \rightarrow 1$, P_{m0} started to increase more quickly. A regression relationship between P_{m0} and N_1/N can be obtained as:

$$P_{m0} = 0.0534 + 0.0139\ N_1/N \quad (\text{cm}^3/\text{g}) \tag{10}$$

or

$$P_{m0} = 0.1150 + 0.0299\ N_1/N \quad (\text{cm}^3/\text{cm}^3) \tag{11}$$

with a regression coefficient $R = 0.970$. The special gravity of mortar was 2.151 g/cm^3 in this study. At failure, the mortar porosity increased by 26%. Also, the volume ratio of mortar to concrete is 0.546, so P_{m0} is equivalent to a porosity in concrete P_{m0}'. Thus Eq. 11 becomes:

$$P_{m0}' = 0.0628 + 0.0163\ N_1/N \quad (\text{cm}^3/\text{cm}^3) \tag{12}$$

Pore Size Distribution

From Figure 1, three obvious peaks of $dP_m/d \log r$ are located at $r = 40$ Å, 370 Å, and 3600 Å, respectively. At these radii, P_m changes sharply (Fig. 2). These P_m values can be crucial for finding the damage mechanisms under fatigue bending. At $r_2 = 370$ Å, the highest peak of $dP_m/d \log r$ occurred and the $dP_m/d \log r$ vs. $\log r$ curve became very spiky, which means that a greater increment of P_m happened here. With increasing loading cycles, this peak height greatly increased. When N_1/N varied from 0 to 1, $dP_m/d \log r$ increased by 33%. The width, however, did not change very much. At $r_1 = 40$ Å, another sub-peak also increased with N_1/N but the peak height was always smaller than that at $r_2 = 370$ Å. The width changed very little even though the peak height increased by 105% when N_1/N varied from 0 to 1. These pores are meso pores. At $r_3 = 3600$ Å, although the peak height was not very big, it

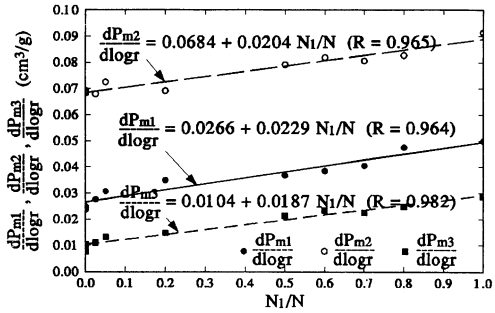

FIG. 4.
Typical differential pore volume of mortar (concrete) at different fatigue stages.

increased by 219% at failure and the width also increased with N_1/N, which means that an even greater increment of P_m might have happened here. The pores with such size are macro pores. $dP_m/d \log r$ vs. N_1/N regression relationships at different radii are obtained as (Fig. 4):

$$\frac{dP_{m1}}{d \log r} = 0.0266 + 0.0229\ N_1/N \qquad (R = 0.964)$$

$$\frac{dP_{m2}}{d \log r} = 0.0684 + 0.0204\ N_1/N \qquad (R = 0.965) \tag{13}$$

$$\frac{dP_{m3}}{d \log r} = 0.0104 + 0.0187\ N_1/N \qquad (R = 0.982)$$

P_m vs. N_1/N regression relations at three $dP_m/d \log r$ peaks can be obtained as (Fig. 3):

$$P_{m1} = 0.0529 + 0.0141\ N_1/N \qquad (R = 0.977)$$

$$P_{m2} = 0.0335 + 0.0133\ N_1/N \qquad (R = 0.981) \tag{14}$$

$$P_{m3} = 0.0084 + 0.0094\ N_1/N \qquad (R = 0.980)$$

Corresponding to these three peaks, $P_{mi}(i = 1, 2, 3)$ increased by 31%, 44%, and 133% at failure, respectively. This means that the volume of macro pores increased much more quickly than meso pores during bending fatigue. Also the incremental P_{mi} are on average 100%, 95%, and 68% of the incremental P_{m0}, which means that the volume change of macro pores contributed mostly to the total porosity change of mortar during bending fatigue.

Porosity of Concrete Using Helium Flow, P_h

Figure 5 shows that the porosity of concrete P_h fairly linearly increased with increasing N_1/N until final fatigue stage. When $N_1/N \rightarrow 1$, P_h started to increase more quickly. A regression relationship between P_h and N_1/N can be obtained as:

$$P_h = 0.1162 + 0.0298\ N_1/N \quad (\text{cm}^3/\text{cm}^3) \tag{15}$$

with $R = 0.979$. At failure, P_h increased by 30%.

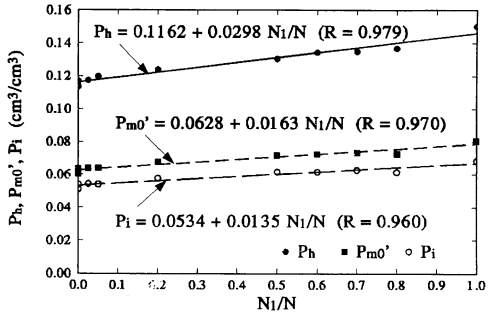

FIG. 5.
Porosity of concrete, mortar and interface at different fatigue stages.

Interface Cavity of Concrete

P_h measured using helium flow can actually be expressed as:

$$P_h = P_{m0}' + P_{ca} + P_i + \Delta P_{mh} \tag{16}$$

where P_{ca} is porosity of coarse aggregate, P_i is interface cavity between cement paste and coarse aggregates, and ΔP_{mh} is the porosity error between mercury intrusion and helium flow methods. Beaudoin (28) found that mercury intrusion and helium flow could be used interchangeably to measure porosity of cement paste if w/c ratio was equal to or greater than 0.40. Based on this, $\Delta P_{mh} = 0$ can be reasonably assumed. Coarse aggregate used in this study was very dense limestone with a very small porosity say 1%, so $P_{ca} \approx 0$ can also be reasonably assumed. From Eqs. 12 and 15, P_i can be approximately obtained as:

$$P_i \approx P_h - P_{m0}' = 0.0534 + 0.0135\ N_1/N \quad (\mathrm{cm}^3/\mathrm{cm}^3) \tag{17}$$

with $R = 0.960$. At failure, P_i increased 25%. Comparison of this value with an increment of 26% in P_m shows that the mortar porosity and the interfacial cavity increased with N/N_1 at a similar rate. In other words, both made similar contributions to the degeneration of concrete under bending fatigue. The latter stands for the propagation of interfacial cracks.

The above research indicates that improving these two phases may help raise fatigue resistance of concrete, such as dense aggregate grading, polymer impregnation, strengthening interface, etc.

Specific Surface Area *S* Using Nitrogen Adsorption

The test data show that specific surface area of mortar from the damaged concrete, S, fairly linearly increased with increasing N_1/N (Fig. 6). A regression relationship between S and N_1/N can be obtained as:

$$S = 1.628 + 1.417\ N_1/N \quad (\mathrm{m}^2/\mathrm{g}) \tag{18}$$

with $R = 0.999$. At fatigue failure, S increased by 85%. However, more tests need to be done to further quantitatively confirm this.

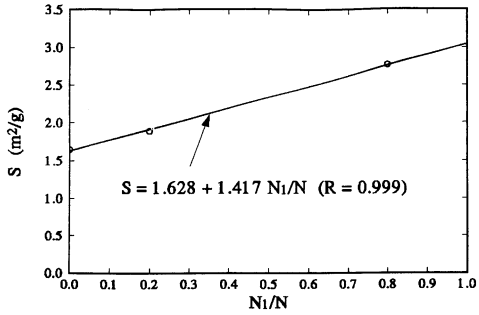

FIG. 6.
Specific surface area of mortar (concrete) at different fatigue stages.

Mean Distribution Pore Size, r_m

r_m is defined as:

$$\log r_m = \frac{\int P(\log r) \log r \, d \log r}{\int P(\log r) \, d \log r} \tag{19}$$

If no continuous $P(\log r)$ is available, r_m can still be numerically determined from:

$$\log r_m = \frac{\sum P(\log r_i) \log r_i \, \Delta \log r_i}{\sum P(\log r_i 0) \, \Delta \log r_i} \tag{20}$$

r_m in Å for mortar calculated from Figure 2 has a good regression relation with N_1/N (Fig. 7) as

$$\log r_m = 2.3808 + 0.0989 \, N_1/N \tag{21}$$

or

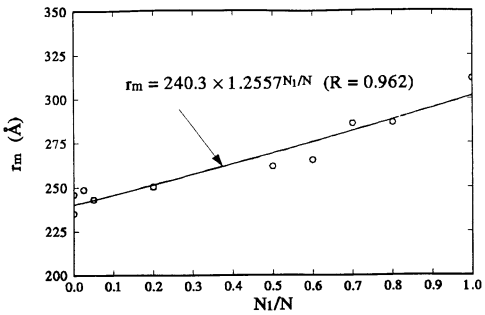

FIG. 7.
Mean distribution pore size of mortar (concrete) at different fatigue stages.

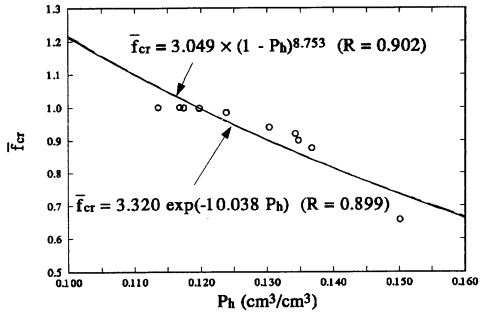

FIG. 8.
Relationship between relative residual strength and porosity of concrete.

$$r_m = 240.3 \cdot 1.2557^{N_1/N} \quad (\text{Å}) \tag{22}$$

with $R = 0.962$. When N_1/N varied from 0 to 1, r_m increased from 240 Å to 310 Å, up by 30%.

Relationship Between Macro and Micro-Meso Properties

The strength and stiffness obtained on macro-materials (f_{cr} and E_c) have very good correlations with the measured micro-meso parameters (P_h and r_m).

The Relationship Between $\bar{f}_{cr}$ and P_h

An exponential $\bar{f}_{cr} - P_h$ relationship is assumed as:

$$\bar{f}_{cr} = \bar{f}_{cr0} \cdot (1 - P_h)^{k_{F1}} \tag{23}$$

where $\bar{f}_{cr0}$ is the relative bending strength at zero porosity or the relative intrinsic bending strength, and k_{F1} is a constant. Using logarithmic regression on 10 sets of test data, $\bar{f}_{cr0}$ and k_{F1} were determined as: $\bar{f}_{cr0} = 3.049$ and $k_{F1} = 8.753$ with $R = 0.902$. A natural exponential expression can also be used here:

$$\bar{f}_{cr} = \bar{f}_{cr0} \cdot \exp(-k_{F2} \cdot P_h) \tag{24}$$

where $\bar{f}_{cr0}$ and k_{F2} were determined using linear regression as: $\bar{f}_{cr0} = 3.320$ and $k_{F2} = 10.038$ with $R = 0.899$. The intrinsic bending strength of concrete f_{cr0} ($P_h = 0$) was at least three times that of the measured modulus of rupture f_r, or $f_{cr0} > 3 \cdot f_r = 23.6$ MPa. The values of f_{cr0}, k_{F1} and k_{F2} obtained in this study are quite close to those by Rößler et al. (6). Equations 23 and 24 are plotted with the test data in Figure 8.

The Relationship Between $\bar{E}_{dB}$ and P_h

An exponential $\bar{E}_{dB} - P_h$ relationship is assumed as:

$$\bar{E}_{dB} = \bar{E}_{dB0} \cdot (1 - P_h)^{k_{E1}} \tag{25}$$

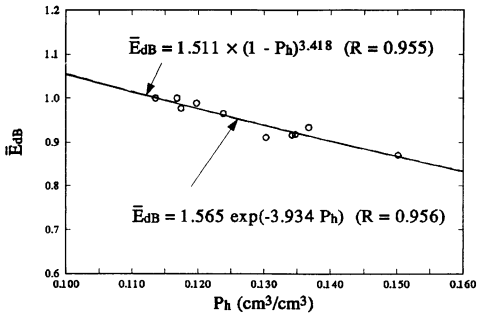

FIG. 9.
Relationship between relative Young's modulus and porosity of concrete.

where $\bar{E}_{dB0}$ is the relative dynamic bending Young's modulus at zero porosity or the relative intrinsic bending Young's modulus, and k_{E1} is a constant. Using logarithmic regression, $\bar{E}_{dB0}$ and k_{E1} were determined as: $\bar{E}_{dB0} = 1.511$ and $k_{E1} = 3.418$ with $R = 0.955$. A natural exponential expression can also be used here:

$$\bar{E}_{dB} = \bar{E}_{dB0} \cdot \exp(-k_{E2} \cdot P_h) \tag{26}$$

where $\bar{E}_{dB0}$ and k_{E2} were determined using linear regression as: $\bar{E}_{dB0} = 1.565$ and $k_{E2} = 3.934$ with $R = 0.956$. The intrinsic bending Young's modulus E_{dB0} ($P_h = 0$) was only about 50% greater than the obtained Young's modulus E_{dB}, or $E_{dB0} \approx 1.5 \cdot E_{dB} = 69.3$ GPa. The fact that $\bar{E}_{dB0}$, k_{E1}, and k_{E2} obtained in this study were smaller than $\bar{f}_{r0}$, k_{F1}, and k_{F2} indicates that the Young's modulus of concrete is less sensitive to porosity than strength. Equations 25 and 26 are plotted with the test data in Figure 9.

The Relationship Between $\bar{f}_{cr}$ and r_m

A natural exponential $\bar{f}_{cr} - r_m$ relationship is assumed as:

$$\bar{f}_{cr} = \bar{f}_{cr0} \cdot \exp(-k_{F3} \cdot r_m) \tag{27}$$

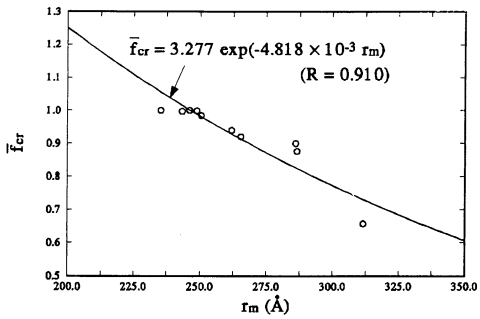

FIG. 10.
Relationship between relative residual strength and mean distribution pore size.

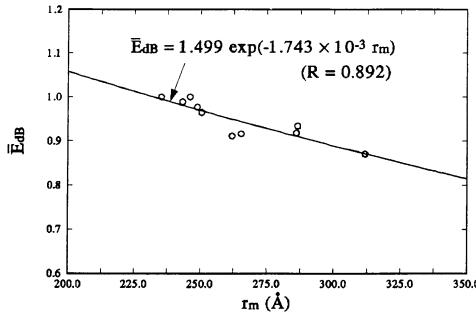

FIG. 11.
Relationship between relative Young's modulus and mean distribution pore size.

Using logarithmic regression, $\bar{f}_{r0B}$ and k_{F3} were determined as: $\bar{f}_{cr0} = 3.277$ and $k_{F3} = 4.818 \times 10^{-3}$ with $R = 0.910$. The intrinsic bending strength f_{r0} ($r_m = 0$) was still at least three times larger than that of the measured modulus of rupture. Equation 27 is plotted with the test data in Figure 10.

The Relationship Between $\bar{E}_{dB}$ and r_m

A natural exponential expression is assumed for $\bar{E}_{dB} - r_m$ relationship:

$$\bar{E}_{dB} = \bar{E}_{dB0} \cdot \exp(-k_{E3} \cdot r_m) \tag{28}$$

Using logarithmic regression on the same sets of test data, $\bar{E}_{dB0}$ and k_{E3} were determined as: $\bar{E}_{dB0} = 1.499$ and $k_{E3} = 1.743 \times 10^{-3}$ with $R = 0.892$. Once again, the intrinsic Young's modulus of concrete E_{dB0} ($r_m = 0$) was about 50% greater than the measured Young's modulus. Similarly, the fact that $\bar{E}_{dB0}$ and k_{E3} obtained in this study were smaller than $\bar{f}_{cr0}$ and k_{E3} still indicates that the Young's modulus of concrete is less sensitive to porosity than is the strength. As mentioned above, r_m is a statistical parameter to reflect micro-meso defects within concrete (pores and interface cracks). From Griffith's classic fracture mechanics, it is easily understood that the strength of concrete significantly depends on micro-defects (23). The Young's modulus of concrete, however, mainly depends on material composition of concrete and individual elasticity and stiffness. Equation 28 is plotted with the test data in Figure 11.

Finally, this study shows that the intrinsic strength and Young's modulus of concrete can also be predicted using damaged concrete with a single composition under different loading cycles rather than using undamaged concrete with varied compositions and curing conditions.

Conclusions

1. This study has shown that the macro characteristics of concrete fatigue damage is the decrease of residual strength and stiffness, but the micro-meso characteristics is the degeneration of pore structure.
2. Porosity, pore size distribution (expressed by mean distribution pore size), and specific surface area can be used as micro-meso damage parameters to evaluate macro damage

of concrete under fatigue bending. The test results show that under bending all the magnitudes of these parameters increased with increasing loading cycles.

3. Porosity of concrete mainly came from mortar pores and interface cavity (cracks). Under bending fatigue, mortar porosity increased at a similar rate as interface cavity in concrete. Development of macro pores ($r = 4000$ Å) contributes mostly to that of the mortar porosity.
4. The experimental results also show good correlations between macro residual properties (bending strength and Young's modulus) and micro-meso parameters (porosity and mean distribution pore size).

References

1. B. Zhang and K. Wu, Cem. Concr. Res. 27, 115 (1997).
2. B. Zhang, D.V. Phillips, and K. Wu, Mag Concr. Res. 48, 361 (1996).
3. B. Zhang, D.V. Phillips, and K. Wu, Mag Concr. Res. 49, 241 (1997).
4. V.S. Ramachandran, R.F. Feldman, and J.J. Beaudoin, CONCRETE SCIENCE—Treatise on Current Research, Heyden & Son Ltd., London, 1981.
5. R.F. Feldman and J.J. Beaudoin. Cem. Concr. Res., 6, 389 (1976).
6. M. Rößler and I. Odler, Cem. Concr. Res. 15, 320 (1985).
7. R.F. Feldman, G.G. Carette, and V.M. Malhotra, Cem. Concr. Compos 12, 245 (1990).
8. D. Winslow and D. Liu, Cem. Concr. Res. 20, 227 (1990).
9. J.J. Beaudoin and V.S. Ramachandran, Cem. Concr. Res. 22, 689 (1992).
10. J.J. Beaudoin, R.F. Feldman, and P.J. Tumidajski, Adv. Cem. Based Mat. 1, 224 (1994).
11. G. Verbeck and R.A. Helmuth, Proc. 5th Inter. Symp. on the Chemistry of Cement (Tokyo), III, 1 (1968).
12. R.F. Feldman, Dura. of Build. Mat. 4, 137 (1986).
13. R.F. Feldman, Fly Ash, Silica Fume, Slag and Natural Pozzolans in Concrete, 2nd Inter. Conf. (Madrid, Spain), ACI SP-91, 973 (1986).
14. J.F. Young, Permeability of Concrete, Inter. Symp. (Detroit, Michigan), ACI SP-108, 1 (1988).
15. D.M. Roy, D. Shi, B. Scheetz, and P.W. Brown, Durability of Concrete, G.M. Idorn Inter. Symp. (Detroit, Michigan), ACI SP-131, 137 (1992).
16. M.Y. Balshin, Dokl. Akad. Nauk. SSSR 67, 831 (1949).
17. E. Ryshkevitch, J. Amer. Ceram. Soc. 36, 65 (1953).
18. K.K. Schiller, Mechanical Properties of Non-Metallic Materials, W.H. Walton, ed., Butterworths Sc. Publ., London, 35 (1959).
19. D.P.H. Hasselmann, J. Amer. Ceram. Soc. 45, 452 (1962).
20. D.P.H. Hasselmann, J. Amer. Ceram. Soc. 46, 564 (1963).
21. I. Odler and M. Rößler, Cem. Concr. Res. 15, 401 (1985).
22. C. Atzeni, L. Massidda, and U. Sanna, Proc. of 1st Inter. Con. on Pore Structures and Materials Properties, Chapman and Hall, 195 (1987).
23. A.A. Griffith, Philosophical Transactions, Royal Society of London, 22, 163 (1920).
24. W. Webull, Fatigue Testing and Analysis of Results, Pergamon Press, London 1961.
25. W. Ding, MSc. Thesis, Dept. of Materials Science and Eng., Tongji Univ., China (1982).
26. Y.Y. Huang, W. Ding, and P. Lu, Mat. Res. Soc. Symp. Proc., Boston, MA, USA, 42 (1984).
27. G. Pons and J.C. Maso, Advanced in Fracture Research (Fracture 84), Proc. of the 6th Inter. Conf. on Fracture (ICF6), New Delhi, India, 2817 (1984).
28. J.J. Beaudoin, Cem. Concr. Res. 9, 991 (1979).